Recovery strategies to cope with micrometeoroid impacts in the LISA mission

Engineering Structures 308 (2024) 117888

Contents lists available at ScienceDirect

Engineering Structures

journal homepage: www.elsevier.com/locate/engstruct

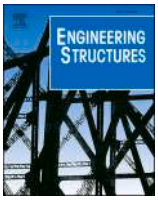

Main factors influencing the shear stiffness of circular joints in tunnel segmental linings analyzed by numerical modelling

Xin Han [a,b], Pierpaolo Oreste [b,*], Fei Ye [a,*]

[a] School of Highway, Chang'an University, Middle-section of Nan'er Huan Road, Xi'an, Shaanxi 710064, PR China
[b] Department of Environment, Land and Infrastructure Engineering (DIATI), Politecnico di Torino, Corso Duca degli Abruzzi 24, 10129 Torino, Italy

ARTICLE INFO

Keywords:
Finite element method (FEM)
Numerical analyses
Tunnel segmental lining
Joint dislocation
Shear stiffness
Circular joint
Back-analysis
Connecting bolt
Interaction analysis
Winkler spring

ABSTRACT

Segmental tunnel lining is a tunnel lining that is adopted when the Tunnel Boring Machine (TBM) is used as excavation machine. It is a concrete lining that is assembled with segments, connected to each other through various devices, including connecting bolts. In order to correctly analyze the behavior of the segmental lining in the longitudinal direction of the tunnel, when actions and loads stress and deform it, it is necessary to know an important mechanical parameter: the shear stiffness of the circular joint. In turn, this fundamental mechanical parameter depends on the behavior of the connecting bolts inside their housing hole. In this work, the behavior of the connecting bolts inside the housing holes was analyzed in detail, through three-dimensional numerical modeling, considering the characteristics of the interaction between the bolt itself and the hole wall, when a relative movement of the lining rings at the circular joint deform the bolt. Thanks to back analysis procedures of experimental laboratory measurements, it was possible to determine the values of some interaction parameters on the bolt-sleeve/concrete interfaces, which are necessary for a correct three-dimensional numerical modeling. The developed numerical model was able to fully describe the behavior of the connecting bolts inside their housing holes and, therefore, also of the circular joint when it is subjected to shear forces that produce the dislocation of the lining rings. The calculation results were compared with experimental measurements obtained from a real-scale tests giving positive results. Thanks to the carried out studies and the developed calculation tool, it is now possible to identify the shear stiffness values of the circular joint with a great detail, in order to evaluate then the mechanical behavior of the segmental lining when subjected to actions and loads (like buoyancy forces due to a liquid filling material around the lining) acting in the longitudinal section of the tunnel.

1. Introduction

The tunnel boring machines (TBMs) is widely adopted during the construction of underground projects in urban areas. However, the segmental lining always has an uneven transversal movement along the longitudinal direction during the construction due to the presence of hydraulic jacks, the backfilling slurry, the compensation grout and the surrounding ground [1-5], of the adjacent underground voids [6,7], and of crossing the strike-slip faulting [8,9]. As a result, the cracking, breakages and leakages can be observed near the joints together with the dislocation between adjacent rings [10-16]: it means that the circular joint has a higher damage risk than the concrete segments [17,18].

Different from a uniform structure, there are obvious bending and shear deformations on circular joints due to their lower stiffness with respect to the stiffness of the concrete segments (Fig. 1). The segmental lining deformation along the longitudinal direction includes two main models: bending model and shear model (dislocation model) [19,12, 20-22]. For the bending model, the main effect of the segmental lining deformation is the opening of the joints (no dislocation between adjacent rings), which depend on the joint bending stiffness. On the contrary, the dislocation is the main feature for the shear model, and is determined by the shear stiffness of the joint correspondingly. From the results of in situ tests on the Royal mail tunnel (RMT) in London (UK) [19,23], an existing cast iron segmental lining tunnel located above a new tunnel, the longitudinal deformation model is composed by the overlapping of the bending and shear models. Based on a 3D numerical simulation along the longitudinal direction of a segmental lining to which buoyance forces were applied, Chen et al. [24] obtained that the main reason of the lining rings uplift is the dislocation deformation over circular joints. Han et al. [25] using a FEM model were able to verify

* Corresponding authors.
E-mail addresses: hanxin@chd.edu.cn (X. Han), pierpaolo.oreste@polito.it (P. Oreste), xianyefei@126.com (F. Ye).

https://doi.org/10.1016/j.engstruct.2024.117888
Received 14 November 2023; Received in revised form 23 February 2024; Accepted 17 March 2024
Available online 10 April 2024

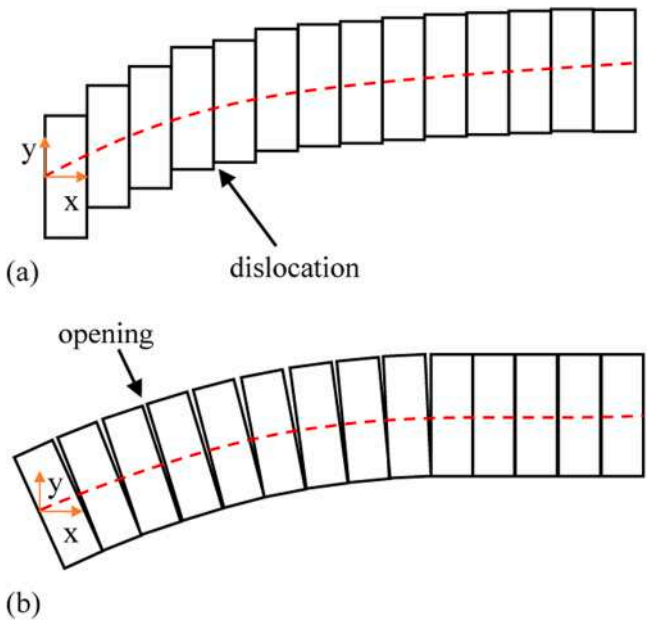

Fig. 1. Deformation schemes of a segmental lining along the longitudinal direction. Key: (a) shear deformation model, (b) bending deformation model.

how the shear stiffness of the circular joint has a great influence on transversal displacements of the segmental lining rings under buoyance forces due to the presence of the slurry (fluid one component filling material) around the lining; moreover the bending stiffness of joints (only affecting rotation angles and moments) has a weak effect on dislocations and transversal displacements [26]. With the increase of the tunnel diameter and a corresponding increase of buoyancy forces acting on the lining [1,3,5], an exact evaluation of the shear stiffness of the joint is fundamental for the evaluation of the longitudinal lining deformation and the containment of the damage risk of the segmental lining.

For understanding the main characteristics of the joint shear deformation, an applied shear force and the corresponding shear displacement were monitored during specific laboratory tests [27-31]. Based on these test results, the process of the shear deformation includes three phases: an initial no sliding phase, on which the static friction on the joint influences the shear deformation; a sliding phase, when tenons and bolts start to go into contact with concrete walls; a final cracking phase, at which cracks develop in the concrete and the bolts tend to yield. Therefore, during the shear deformation of the circular joints, bolts and tenons have a significant role.

For the bolt shear performance many detailed tests have been carried out and are described in the scientific literature [32-37]; moreover, some analytical methods were specifically developed and are available [33,38-41]. However, there is a great difference in the behavior of the bolt used to connect concrete segments of a lining with respect to the one adopted to reinforce the rock mass or a concrete structure: indeed the gap existing between the connecting bolt and the hole wall can cause the change of the contact area varying the relative transversal displacement between adjacent segments.

The analysis of the joint shear deformation is based on the evaluation of the shear stiffness of a circular joint. A simplified approach considers the joint shear stiffness as the shear stiffness of the segmental lining ring multiplied by a reduction factor [42]. Considering the influence of the bolt on the joint, a new equation of the joint shear stiffness is proposed by Wu et al. [20], which was then updated and widely used by researchers [43,44,12,45,46].

However, the equation developed by Wu et al. [20] is based on the consideration that the shear stiffness of a joint is represented by the shear stiffness of its connecting bolts; it leads to overestimating the joint shear stiffness since it ignores the interaction between the bolt and the hole wall. In fact, the shear deformation of the joint is determined not only by the connecting bolt shear deformation but also by the compression reaction of the concrete hole wall in contact with the bolt. Based on the Timoshenko beam theory, Han et al. [47] developed a FEM model to evaluate the shear deformation of a straight bolt and of a curved one, installed in a hole, considering the influence of the concrete compression on the hole wall; furthermore, the shear deformation of an inclined bolt was evaluated in detail, and a simplified calculation method was proposed [48]: the foundation modulus of the concrete hole wall was identified as a critical parameter for evaluating the interaction between the bolt and the concrete hole wall. Although the foundation modulus of the concrete has been tested by various researchers [49-51], a great differences among the test results is evident. In order to quickly evaluate the shear deformation and also the shear stiffness of a circular joint, which is a key parameter when analyzing the segmental lining deformation along the longitudinal direction, the concrete foundation modulus needs to be discussed and analyzed with more detailed.

When the beam theory to analyze the shear deformation of a bolt in a concrete hole is adopted, springs are used to simulate the reaction force from the concrete hole wall to the bolt: the spring stiffness can be determined on the basis of the concrete foundation modulus, which represents a reaction characteristic of concrete under the application of a unitary concentrated force [47,48]. Furthermore, the foundation modulus can be divided into a normal (compressive) foundation modulus and a shear one: they are related to a normal deformation and a shear deformation of a concrete surface.

The numerical 3D model can consider a segmental lining joint with more detail and it can be used to analyze the joint shear stiffness, considering the influence of the tunnel size and of the material parameters.

In order to further evaluate the joint shear stiffness, the concrete deformation under the movement of a bolt at a contact with it was studied and discussed in this paper. Firstly, the main equations which are adopted to calculate the concrete compressive foundation modulus and are available in the scientific literature are presented, and the laboratory tests specifically developed for the evaluation of the concrete compressive foundation modulus are analyzed. Based on the test results, some numerical models are developed to determine the material parameters by a back analysis procedure; the concrete compressive foundation modulus is calculated and compared with the one from the most commonly used equations. Furthermore, the relative shear deformation between the bolt and the bolt hole is analyzed and the concrete shear foundation modulus is analyzed. Finally, a developed 3D model of the circular joint with an inclined bolt is developed to simulate the bolt deformation in the concrete hole wall when the segments have a relative transversal movement along the joint.

2. The interaction between the bolt and concrete in the scientific literature

2.1. The main equations for the calculation of the concrete compressive foundation modulus

With respect to the interaction between the bolt and the concrete hole wall, the compressed interaction is discussed deeply. The compressed interaction between the bolt and the concrete can be represented by the concrete compressive foundation modulus which is influenced by the materials strength and the contact area between the bolt and the concrete. The methods that are adopted to analyze the concrete compressive foundation modulus k_c can be divided into two types: the compression method and the shear method, and the corresponding test schemes for two methods are shown in Fig. 2.

The compression method was carried out by Soroushian et al. [50], and the following equation was suggested to calculate the concrete compressive foundation modulus.

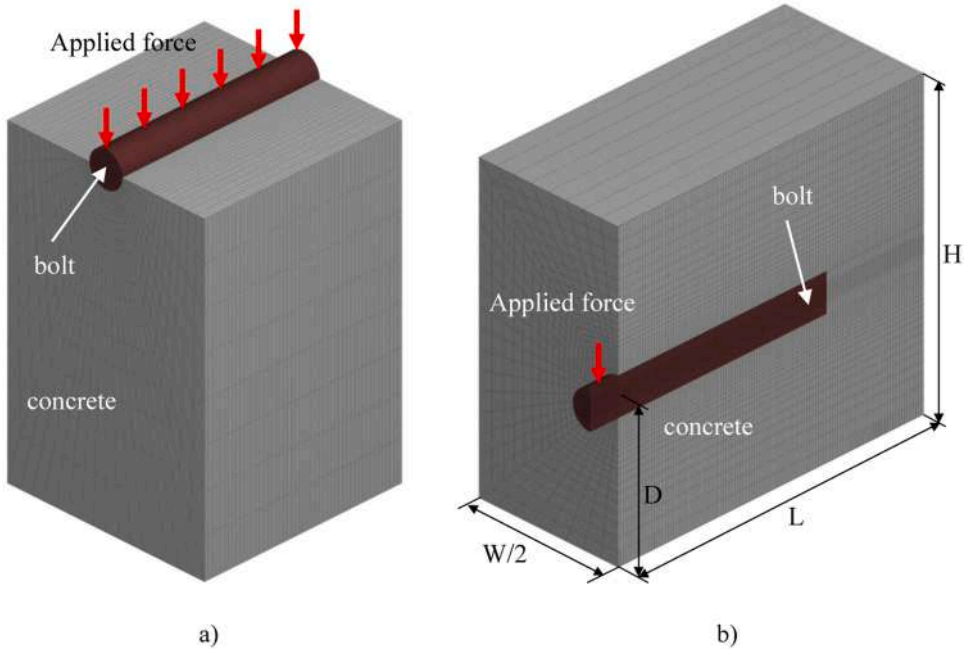

Fig. 2. Methods for the evaluation of the concrete compressive foundation modulus. Key: (a) the scheme of the compression method; (b) the scheme of the shear method.

$$k_0 = \frac{127 \bullet f_{cc}^{0.5}}{(d_b)^{\frac{2}{3}}} \tag{1}$$

Where f_{cc} is the concrete cylindrical compression strength (MPa); d_b is the bolt diameter (mm); the unite of the concrete compressive foundation modulus k_0 is MPa/mm, and the units of the above three parameters is also adopted in the following empirical equations (Eqs. (6), (9), (10) and (12)).

The compression method can directly evaluate the concrete compressive foundation modulus, but the above developed equation is only validated to be able to evaluate the concrete foundation modulus for high levels of load [52]. When the load is small, the concrete can appear stiffer.

The shear method is an indirect one, and rely on the mathematical model of a beam on an elastic and cohesionless foundation (BEF model), which is widely adopted to evaluate the dowel action of steel bars embedded in a concrete structure [53–59,52,60–63,51].

For the BEF model the relationship between the applied force and the related vertical displacement of the bolt head (where the force is applied) can be represented by the following equation [64]:

$$y_d = \frac{V_d}{2 \bullet \alpha^3 \bullet E_b \bullet I_b} \bullet (1 + \alpha \bullet d_l) \tag{2}$$

where y_d is the vertical displacement of the bolt head when the force V_d is applied, E_b is the elastic modulus and I_b is the inertia area moment of the bolt, d_l is the distance between the location of the applied force and the concrete boundary, α can be obtained by the following equation:

$$\alpha = \sqrt[4]{\frac{k_c \bullet d_b}{4 \bullet E_b \bullet I_b}} \tag{3}$$

where k_c (MPa/mm) is the concrete compressive foundation modulus, and was analyzed based on different test results, but it shows a great scattered distribution from 75 MPa/mm to 1244 MPa/mm [52,50,65].

Considering the influence of the concrete damage and the bolt yielding, the concrete compressive foundation modulus k_c can be calculated starting from the initial value k_0 and considering a damage index ω [52].

$$k_c = \omega \bullet k_0 \tag{4}$$

Based on the equation (Eq. (1)) of Soroushian et al. [50], Poli et al. [52] suggested the following equation as the damage index based on the applied force V_d on the bolt head:

$$\begin{cases} \omega = 2.12 & V_d/V_u \le 0.4 \\ \omega = [0.544 + 0.026 \bullet \cosh(8 \bullet (V_d/V_u - 0.4))]^{-4/3} & V_d/V_u > 0.4 \end{cases} \tag{5}$$

where V_u is the maximum value of the applied force on the bolt head during the laboratory test when the concrete block tends to be failed under the application of the bolt.

Furthermore, Poli et al. [52] also developed a new equation for the initial value of concrete compressive foundation modulus k_0 and the damage index ω based on the displacement of the bolt head:

$$k_0 = \frac{600 \bullet f_{cc}^{0.7}}{d_b} \tag{6}$$

$$\omega = \left[1.5 \bullet \left(a + \sqrt{d^2 \bullet \left(40 \bullet \frac{y_d}{d_b} - b \right)^2 + c^2} \right) \right]^{-4/3} \tag{7}$$

where a, b, c and d are the coefficients and can be estimated as follows:

$$\begin{cases} a = 0.59 - 0.011 \bullet f_{cc} \\ b = -0.23 + 0.0075 \bullet f_{cc} \\ c = 0.44 + 0.0038 \bullet f_{cc} \\ d = 0.58 + 0.0025 \bullet f_{cc} \end{cases} \tag{8}$$

Figueira et al. [53] reevaluated k_0 on the basis of the experimental results of Poli et al. [52], and modified the coefficients a, b, c and d of Eq. (7):

$$k_0 = \frac{700 \bullet f_{cc}^{0.7}}{d_b} \tag{9}$$

On the other side, Maekawa and Qureshi [56] developed an empirical equation for the concrete compressive foundation modulus based on the indoor test results.

$$k_0 = \frac{150 \bullet f_{cc}^{0.85}}{d_b} \tag{10}$$

Maekawa and Qureshi [56] considered that the bolt is on the elastic behavior when the bolt has a small displacement and taken three times of the length from the location of the maximum bending moments to the interface as the influenced length L_{co} of the steel bar when the bar is on the elastic phase. Furthermore, considering the nonlinear behavior of both the steel bar and concrete with the increasing of bolt movement related to concrete wall, developed the following piecewise function to calculate the influenced length L_c based on an damage index $DI = (1 + 150 \bullet S/d_b)/(y_d/d_b)$, where the bolt movement along the perpendicular direction is considered (y_d/d_b) and S is the axial displacement of the bolt at the interface.

$$\begin{cases} L_c = L_{co} & DI \le 0.02 \\ L_c = L_{co} \bullet \left[1 + 3 \bullet (DI - 0.02)^{0.8}\right] & DI > 0.02 \end{cases} \tag{11}$$

On the basis of the results of Maekawa and Qureshi [56], Moradi et al. [59] derived the equation for the concrete compressive foundation modulus:

$$k_0 = \frac{220 \bullet f_{cc}^{0.85}}{d_b} \tag{12}$$

$$\begin{cases} \omega = 1 & DI_{sim} \le 0.02 \\ \omega = \dfrac{1}{\left[1 + 3 \bullet (DI_{sim} - 0.02)^{0.8}\right]^4} & DI_{sim} > 0.02 \end{cases} \tag{13}$$

where the damage index ω can be calculated simply by $DI_{sim} = (y_d/d_b)$, and only the shear displacement y_d is considered.

It can be stated that the concrete compressive foundation modulus depends on the strength of concrete and on the diameter of the bolt: however it turns out to be inconsistent among the cited references.

An important characteristic is the variability of the value with the deformation of the bolt, which is caused by the crush of the concrete under the application of the force by the bolt [52]. Therefore, the accurate determination of the concrete strength under the application of the bolt is important to determine the concrete compressive foundation modulus.

Secondly, under the application of the bolt partial load, the concrete bearing capacity also depends on the contact area [52]. Therefore, the contact area between the bolt and the concrete is another key parameter for the foundation modulus of the concrete and the bolt deformation.

Finally, the bolt deformation on the bolt hole depends on the interaction between the bolt and the hole wall. Due to the existence of a gap between the bolt and the hole, the foundation modulus of the concrete is also influenced by the gap, which depend on the difference in the diameter of the hole and of the bolt.

In order to accurately analyze the concrete compressive foundation modulus, the strength of the concrete under the partial load of bolt need to be discussed further.

2.2. Test results for the bolt compression deformation on a concrete surface

Compression method tests [49,50] mainly focuses on the limit condition of the bolt-concrete interaction. The tests with the shear method [54,56,58,52,65] are more common; in Fig. 3 some available results in terms of applied force-bolt head displacement are shown (the main mechanical and geometrical parameters of the bolt and concrete are shown in Table1).

where the sizes W×H×L are the width, height and length of the concrete block and D is the distance of the bolt axis from the bottom of the block (Fig. 2).

From the results of Fig. 3, it is possible to see how most of the applied load-bolt head displacement curves are located on a specific range;

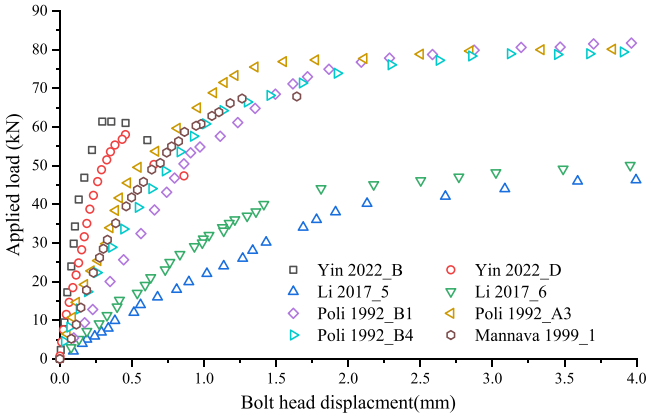

Fig. 3. The test results of the bolt head displacement under the application of a force (shear method). Key: **Yin 2022_B** means that the case is from the literature of Yin et al. [65], and the No. of the special cases on the reference is **B**.

moreover there is an obvious nonlinear trend during the test. Since the slope of the curves can refer to the concrete compressive foundation modulus, it tends to decrease with the increase of the displacement value due to the concrete crushing and the bolt yielding.

Comparing the different results, the ones from Li et al. [54] show a more soft behavior. The main difference of Li et al. [54] tests with reference to the others is the D length (Fig. 2). On the contrary, the results of Yin et al. [65] show a more stiff behavior. In addition, there are no reinforced bars in the concrete for the cases of Li et al. [54] and Yin et al. [65]: any influence of the reinforcing bars in the concrete is therefore avoided. Considering that the case from Yin et al. [65] is more close to the results arising from the other cases, it was chosen to analyze in the detail the parameters of the concrete and the bolt in the next sections of the paper.

2.3. The scale effect of concrete and the back analysis procedure to obtain mechanical parameters

Under the application of a partial load on a concrete block, crushing damage and splitting cracks can be observed [66], where the surrounding concrete has a limitation on the damaged block as shown on Fig. 4, which cause a scale effect on the concrete. The scale effect of concrete has a significant influence on its behavior: concrete can bear a higher compressive load when the force is applied on a small area; it increases with the decrease of the loaded area [67]. Therefore, the compression strength of the concrete under the application of a partial load needs to be evaluated based on test results.

Since the diameter of the bolt is small, the contact area between the bolt and concrete on the hole wall is also very small. For this reason the materials parameters need to be determined on the basis of the test results using a back analysis procedure. A complete back analysis procedure always includes the following aspects [69]:

(1) A representative calculation model: this model can be a complex numerical model or also a simplified analytical one, where the input parameters include the target back-analysis parameters, and one of the output values can be compared with the test results directly.
(2) An error function: the function can be used to show the distance between the calculated results and the test measurements.
(3) An optimization algorithm: the algorithm can be used to efficiently find the new input parameters in order to reduce the difference of the calculation results from the tests measurements.

The complete back analysis with a sophisticated optimization algorithm is always useful for simple analytical models with short

Table 1
Main mechanical and geometrical parameters of the bolt and concrete for the shear tests available in the scientific literature.

Bolt				Concrete				References
Type	Yielding strength (MPa)	Diameter (mm)	Length (mm)	Yielding strength (MPa)	W×H×L (mm ■ mm ■ mm)	D (mm)	Reinforced bars	
Ribbed bar	432	24	400	40	300 × 200 × 400	100	Yes	Poli et al.[52]
Plain bar	400	25.4	250	40	381 × 254 × 381	127	/	Mannava et al.[58]
Ribbed bar	400	25	400	50	300 × 250 × 400	177.5	No	Li et al.[54]
Plain bar	235	25	150	50	200 × 200 × 220	100	No	Yin et al.[65]

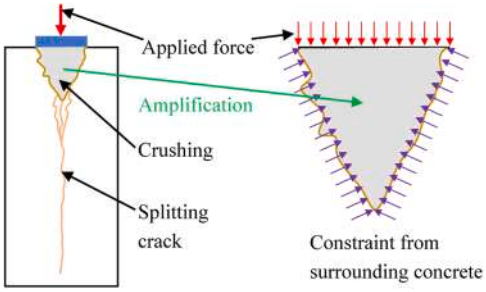

Fig. 4. The crushing damage and splitting cracks in a concrete block under the application of a partial load on a surface. The figure is based on the test results from Conforti et al. [66] and Markić et al. [68].

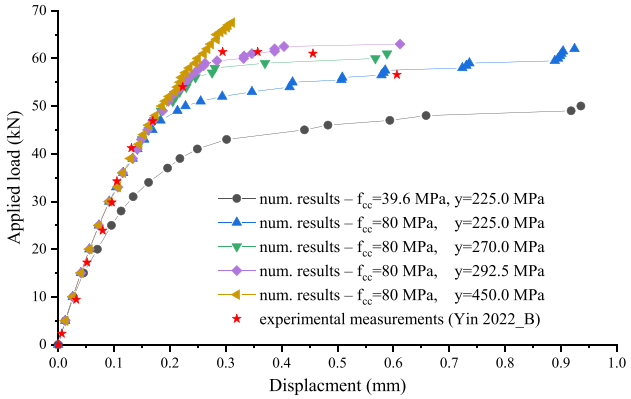

Fig. 5. The comparison of the calculation results (assuming an elastic-plastic behavior for both concrete and bolt steel) with laboratory test measurements [65] in the final step of the back analysis procedure (trial-and-error approach). Key: f_{cc} is the compressive strength of concrete (cylindric sample); σ_y is the yielding stress of steel; Yin 2022_B means the test B developed by Yin et al. [65] (Fig. 2b).

calculation times; while a trial-and-error approach is usually adopted to carry out the back analysis for complex numerical models with time-consuming calculations [70]; the trial-and-error approach consists of adjusting the input parameters on the basis of the continuous comparison of the calculation results with the in situ measurements.

3. The evaluation for the compression deformation of the bolt in the concrete hole

3.1. A preliminary evaluation of mechanical parameters for concrete and the bolt

The laboratory test of Yin et al. [65] (Table 1 and Fig. 2b) was simulated by a numerical tridimensional model in order to study the bolt shear deformation in a concrete block. The back analysis procedure was developed in order to find the representing values of the main mechanical parameters for the bolt steel and concrete at a very small scale in the bolt-concrete interaction. The bolt steel and concrete were considered with an elastic and perfect plastic behaviour. Various changes have been made to the mechanical characteristics of the materials and in particular to the compressive strength of concrete (f_{cc}) and the tensile strength of steel (σ_y) adopting the trial-and-error approach. The final solution of the back analysis made it possible to identify the combination of input parameters that is able to minimize the error between the measurements obtained from the laboratory experimentation [65] and the results of the numerical calculation using the Flac3D code (Fig. 5). In the specific examined case, the solution that best approximates the experimental measurements is the one represented by the purple line (Table 2): f_{cc}= 80 MPa, σ_y = 292.5 MPa.

Table 2
Mechanical parameters for concrete and the bolt steel obtained at the end of the back analysis procedure.

Parameters of Concrete	Value	Parameters of steel (bolt material)	Value
Elastic modulus (GPa)	35	Elastic modulus (GPa)	200
Poisson's ratio	0.2	Poisson's ratio	0.3
Compression strength (MPa) (f_{cc} for the cylinder sample)	80	Tensile Yielding strength (MPa) (σ_y)	292.5
Tensile strength (MPa)	3.5	-	-
Friction (°)	41	-	-

3.2. The evaluation of the compressive deformation of the bolt hole on its cross section

In order to analyze the concrete compressive foundation modulus on the hole wall, a specific numerical model was developed (Fig. 6); this model allows to study the type of reaction of the hole wall when the bolt moves in contact with it due to the relative displacement at the circular joint between two adjacent rings of the segmental lining. In the central part of the model the cross section of the hole is represented with the cross section of the bolt inside. Different hole diameters were considered in the calculation, keeping the bolt diameter constant and equal to 30 mm. The adopted mechanical parameters for concrete and the bolt steel were the ones obtained by the back analysis procedure shown in the previous section.

The displacements of the bolt axis were monitored in the model and the concrete compressive foundation modulus (k_{c_num}) was calculated by the following equation:

$$k_{c\_num} = \frac{F_{applied}}{d_b \bullet l_{width} \bullet s_{bolt}} \tag{14}$$

where $F_{applied}$ is the applied force to the bolt, l_{width} is the width of the model along y-axis (perpendicular to the considered transversal section), s_{bolt} is the displacement of the bolt under the application of the applied force $F_{applied}$.

The calculated values of k_{c_num} varying the applied force are shown in Fig. 7.

In Fig. 7, the concrete compressive foundation modulus k_{c_num} shows a decrease trend with the increase of the applied force. When there is a gap between the bolt and the hole wall, the concrete compressive

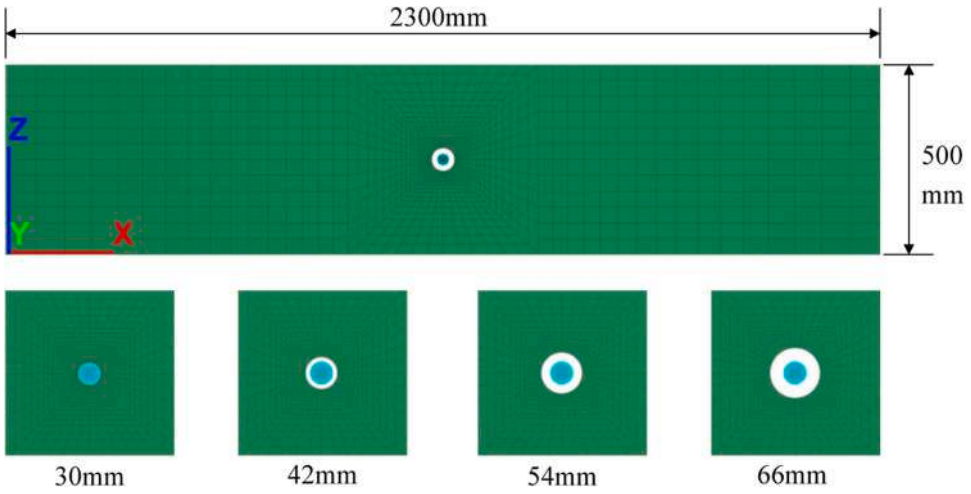

Fig. 6. Numerical model of the transversal section of the bolt in the bolt hole in order to evaluate the compressive reaction of concrete when the bolt (diameter 30 mm) moves at a contact with it. Key: 30 mm, 42 mm, 54 mm and 66 mm are the considered value of the hole diameters. The height of the model is equal to a typical value of the thickness of the segments (500 mm); the length is about four times of the thickness value.

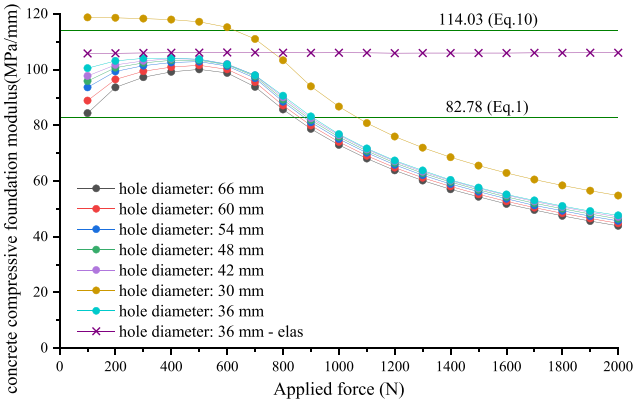

Fig. 7. Calculated values of the concrete compressive foundation modulus (k_{c_num}) varying the force applied to the bolt, for different hole diameters (bolt diameter 30 mm). For a hole diameter of 36 mm, the case of both concrete and the bolt steel with an elastic behavior was also performed. Key: two different values of k_{c_num} were also calculated (horizontal lines) using Eqs. (1) and (10).

foundation modulus is smaller than the one of the no gap condition: the existence of the gap produces a reduction of k_{c_num} and the bigger hole diameters have a lower value.

The development of the plastic zone around the bolt is shown in Fig. 8: at the early stage (for low values of the applied force) only a little zone around the bolt is plastic, then the plastic zone develops till to reach the bottom boundary with an increase of the applied force.

The height of the compressed zone needs to be considered further when the concrete compressive foundation modulus is evaluated. Therefore, the influence of the location of the bolt in the cross section was studied and the results of the numerical calculation are shown in Fig. 9; the plastic zones in the concrete around the bolt are shown in Fig. 10 for the case of an applied force to the bolt equal to 1000 kN.

The curves of the concrete compressive foundation modulus in Fig. 9 show a similar trend when the applied force is small; with the increase of the applied force, the concrete compressive foundation modulus starts to decrease after a phase where it is constant. The height of the compressive zone (distance of the hole axis from the model bottom) has a great influence on the stiffness: when the height is small, a lower concrete compressive foundation modulus can be found. The development of plastic zones around the hole (Fig. 10) is mostly due to tensile failure.

When the bolt is in the lower location (distance from the bottom 50 mm), there is a larger plastic zone; with the increase of the distance the plastic zone around the bolt decrease, but there is no significant reduction of the plastic zone on the bottom side of the model: the main reason is the bending deformation in that zone which leads to a tensile deformation along the bottom side of the sample. On the contrary, the plastic zone around bolt hole is due to the crush of the concrete under the application of the compression force from bolt. When the bolt is close to the bottom boundary, the combination of the two types plastic zones obviously reduces the loading capacity of the concrete block and the concrete compressive foundation modulus.

The possible presence of reinforcement bars in the concrete is not considered in the numerical models: steel bars can improve the tensile strength of the concrete structure.

Based on the Figs. 7 and 9, on the elastic phases of the materials, the calculated results of the concrete compressive foundation modulus are located in the range determined by the values calculated from Eqs. (1) and (10). Otherwise, the development of the plastic zone on the bottom of the concrete block can be improved by the reinforced bars. Therefore, the value of the concrete compressive foundation modulus can be determined approximately by the Eqs. (1) or (10).

4. Evaluation of the shear deformation of bolt-sleeve/concrete interface

The shear foundation modulus of the composite bolt-sleeve/concrete interface on the thread part of the bolt (Fig. 11), is influenced by the presence of the sleeve.

A detailed tridimensional numerical model (Flac3D) on the basis of a laboratory experiment developed by Geng et al. [71], was developed (Fig. 12). The width, length and height of the concrete block are 550 m × 550 m× 500 mm; the length of the M40 bolt is 700 mm, including a shank part (480 mm) and a thread one (220 mm). The material parameters are shown in Table3.

In the numerical model, an interface is introduced to simulate the shear deformation of the composite structure. During the simulation of the bolt tensile deformation, the bonded slip model is adopted; it allows the interface having a relative slip when the interface keep intact [72]. In the developed model, the normal stiffness of the interface has a small influence on the bolt tensile deformation. Instead the shear stiffness and the cohesion of the interface are the main parameters influencing the tensile deformation of the bolt.

In order to evaluate the shear stiffness of the interface, a simplified

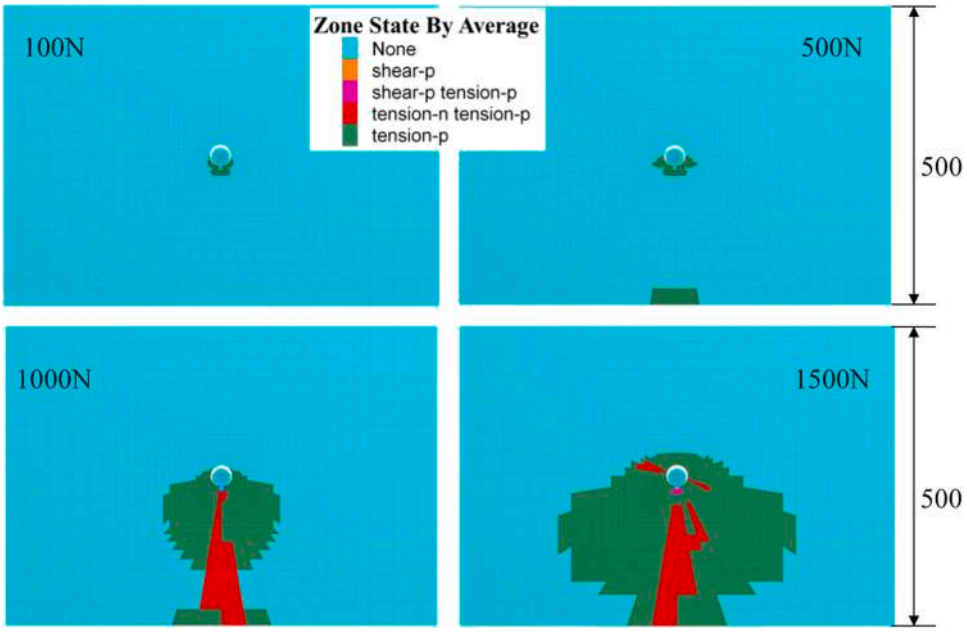

Fig. 8. Plastic zones in the concrete around the hole for the case of a hole diameter 36 mm (bolt diameter 30 mm). Key: 100 N means the value of the vertical force (downward) applied to the bolt.

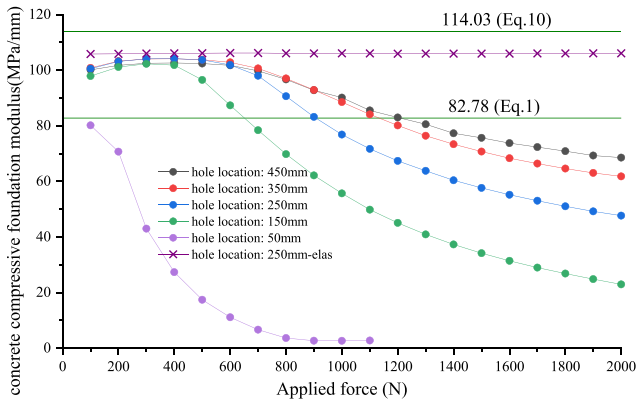

Fig. 9. Calculated values of the concrete compressive foundation modulus (k_{c_num}) varying the force applied to the bolt (diameter 30 mm), for different hole locations (location means the height of the hole axis from the bottom of the concrete block). For a hole location of 250 mm, the case of both concrete and the bolt steel with an elastic behavior was also studied. Key: two different values of k_{c_num} were also calculated (horizontal lines) using Eqs. (1) and (10).

method is developed, which can give the shear foundation modulus of the composite structure based on laboratory test result, and the detailed procedure for deriving the equation can be found in Han et al. [48].

On the basis of the test results, the tensile stiffness can be obtained by the ratio between the applied tensile axial force N_0 and the relative axial displacement of the bolt head v_0 (Fig. 12):

$$K_{s,t} = \frac{N_0}{v_0} = \frac{E \bullet A_b}{\frac{\coth(\rho \bullet l_{thread})}{\rho} + l_{shank}} \tag{15}$$

where E is the elastic modulus of the bolt steel, the parameter ρ can be calculated from the shear foundation modulus of the composite structure:

$$\beta_c = \frac{\rho^2 \bullet E \bullet d_b}{4} \tag{16}$$

According to Eqs. (15) and (16), the shear foundation modulus is equal to 10.1 MPa/mm based on the test results of Geng et al. [71]. Having evaluated from the pullout test a sleeve strength of the concrete structure equal to 835 kN, a cohesion of 30.2 MPa was determined based on the length of the thread part and the diameter of the bolt. The normal stiffness of the interface was evaluated 10Gpa. The numerical modelling results and test measurements are compared in Fig. 13 for the case that the length of the installed bolt is 70% of the length of the thread part.

How is possible to see in Fig. 13, the interface doesn't yield, and the curves increase as the black lines in Fig. 13 when the shear strength is 835 kN. However, for the lower shear strength(250 kN) and for the in-situ measurement, the curves yield which drift away from black lines and go to the plastic phase. The curves of the lower shear strength and the in-situ measurement can be divided into two phases: an elastic phase and a plastic one. In the elastic phase, the test measures have a good agreement with the numerical result (the inclined angles of the lines depend on the shear foundation modulus, which is calculated by Eqs. (15) and (16)). Therefore, the same two equations can be used to evaluate the shear foundation modulus of the interface of bolt-sleeve/concrete. If there is not any available test result, the value obtained by Geng et al. [71] (10.1 MPa/mm) can be considered as a reference value.

In the second phase, the numerical results tend to be described by a horizontal line (constant force increasing the axial displacement).

The state condition and shear stresses in the interface are shown in Fig. 14 when the applied axial forces were equal to 228.7 kN and 246.2 kN. Although the adopted shear strength was 250 kN (it means a cohesion of the interface equal to 12.915 MPa), the interface yields below this value of the applied force: the main reason is that the distribution of the shear stress along the interface is not uniform under the influence by the boundary effect. The whole interface tends to yield when the applied tensile force increases of 17.5 kN, as can be seen in Fig. 14a and b. Furthermore, the plastic zone developed around the bolt, has a small influence on the bolt tensile deformation; however, the trend axial force-axial displacement is not linear (reference to the red dotted straight line in Fig. 13).

As regards the cohesion of the bolt-sleeve/concrete interface, from the back-analysis of the measurements carried out in the experimentation of Geng et al. [71], a value of approximately 14.7 MPa has been identified based on the average value (281.22 kN) of the tensile force in Fig. 13 and considering the case that the length of the installed bolt is

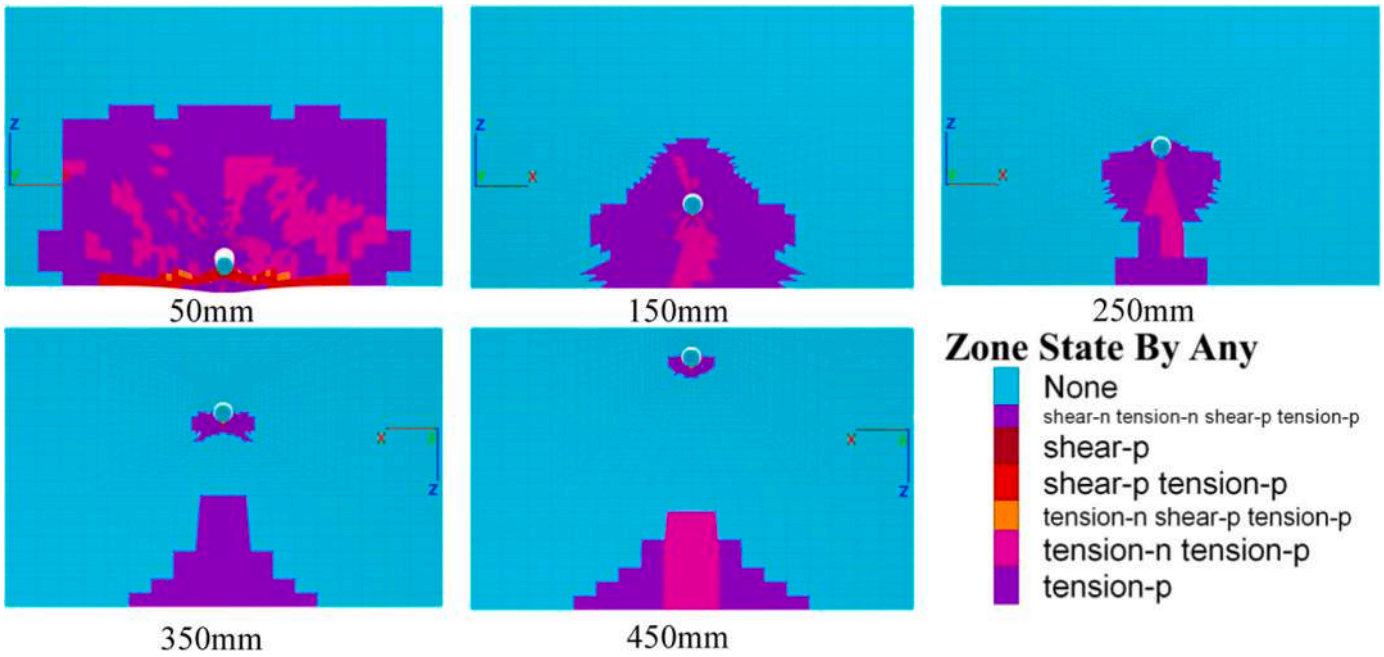

Fig. 10. Plastic zones in the concrete around the hole for the case of a hole diameter 36 mm (bolt diameter 30 mm) and of applied force to the bolt equal to 1000 kN, varying the hole location (distance of the hole axis from the bottom of the model). Key: 50 mm means the distance of the hole axis from the bottom of the model.

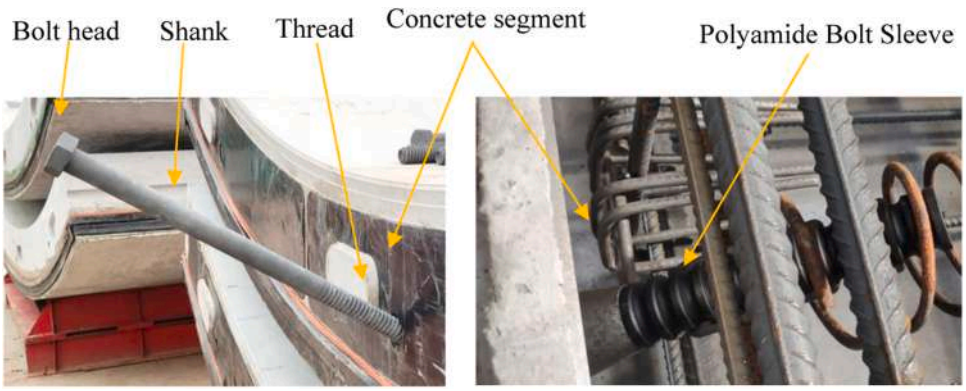

Fig. 11. The typical structure of an inclined bolt crossing a circular joint after [48].

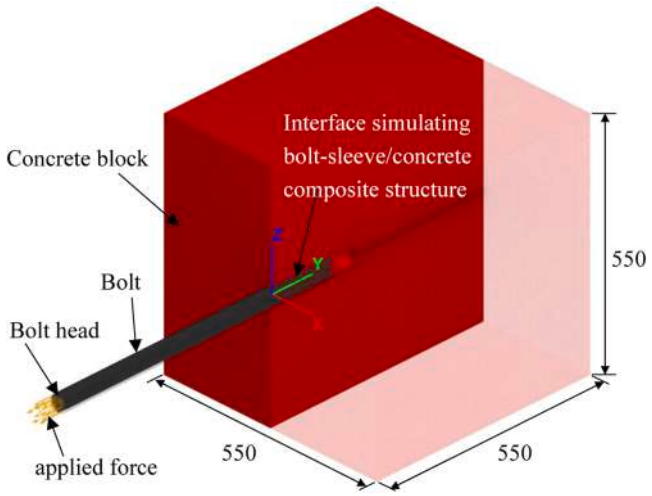

Fig. 12. Tridimensional numerical model to simulate the bolt tensile test of Geng et al. [71] in the concrete hole (lengths in mm).

Table 3
Main parameters of the steel bolt and concrete in the numerical model simulating the bolt tensile test of Geng et al. [71].

Material	Young's Modulus (GPa)	Poisson's ratio	Cohesion (MPa)	Friction (°)	Tensile strength (MPa)
Bolt	210	0.3	450	-	900
Concrete	37	0.2	18.23	41	4.1

100% of the length of the thread part on the test of Geng et al. [71]. This value was considered representative for the particular connection between the terminal area of the bolt and the surrounding concrete, regardless of the diameter of the bolt itself.

5. Detailed model of an inclined connecting bolt using tridimensional numerical model

The 3D numerical model can be used to study in the behavior of an inclined connecting bolt and the interaction between the bolt and concrete in order to evaluate the shear deformation of a circular joint. A

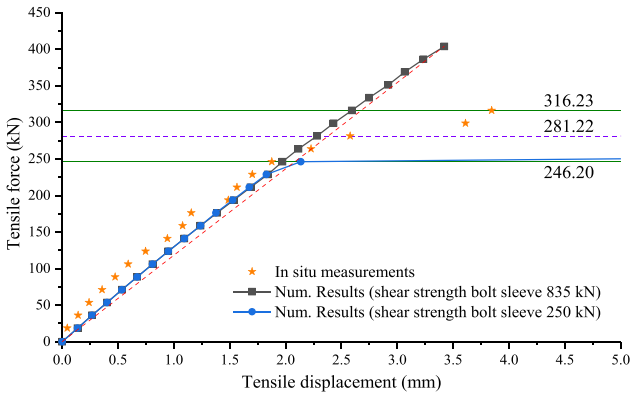

Fig. 13. Comparison between test measurements by Geng et al. [71] and numerical modelling results for the case that the length of the installed bolt is 70% of the length of the thread part.

specific reference case was analyzed [27]: the tunnel lining had an external and inner diameters of 11.8 m and 10.8 m, respectively, and a width of the ring of 2 m; the connection with the adjacent rings is made by 46 M30 inclined bolts along the circular joint. A Flac3D numerical model was prepared to simulate the joint shear deformation with the inclusion of an inclined bolt. The size of the model and the parameters of the bolt and bolt hole are shown on Fig. 15. In order to represent the correct interaction between the different elements of the model, five interfaces were added to the surface of the bolt and sleeve (Fig. 15): interfaces A, B and D are used to transfer the normal force between adjacent structures (the adopted normal stiffness is 100,000 GPa and the shear stiffness 0); interface E is attached to the bottom surface of segment 1 (the friction is ignored on the contact surface between the two segments, the normal stiffness is again equal to100000GPa, and the shear stiffness is equal to 0); interface C represents the properties of the interface of bolt-sleeve/concrete (Table 4); the material parameters of the bolt and concrete are listed in Table5, obtained on the basis of the back analysis results of Sect.3.1.

During the shear test, the segment 2 is fixed on two of its sides along the directions of axes x and y; the bottom of the segment 2 is also fixed. A uniform distribution of the force is applied on the two boundaries along the x-axis direction as shown in Fig. 15 (the movement of the segment 1 along the y and z axes are equal to 0).

When the segment 1 has a relative displacement with segment 2, there are two different directions: along the positive and negative x-axis direction. When segment 1 has a movement along the negative x-axis direction, the bolt is stretched and the bolt head is compressed by the bolt hole of the segment 1; otherwise, there is no tensile stress in the bolt. Therefore, there are two different characterizing types of the deformation behavior of the inclined connecting bolt: tensile and no-tensile behavior. Both of the two behaviors were studied by the tridimensional numerical model. The state condition of concrete and of the bolt is shown in Fig. 16, with the representation of plastic zones in the numerical model. Furthermore, the state condition of the bolt is shown in Fig. 17 when the movement of the segments produces a tensile behavior and no-tensile behavior of the bolt; the test results by He et al. [27] are also added to the Fig. 17.

In Fig. 16, there is an obvious difference between the two models. When the bolt is stretched (tensile behavior), the yielding of the joint

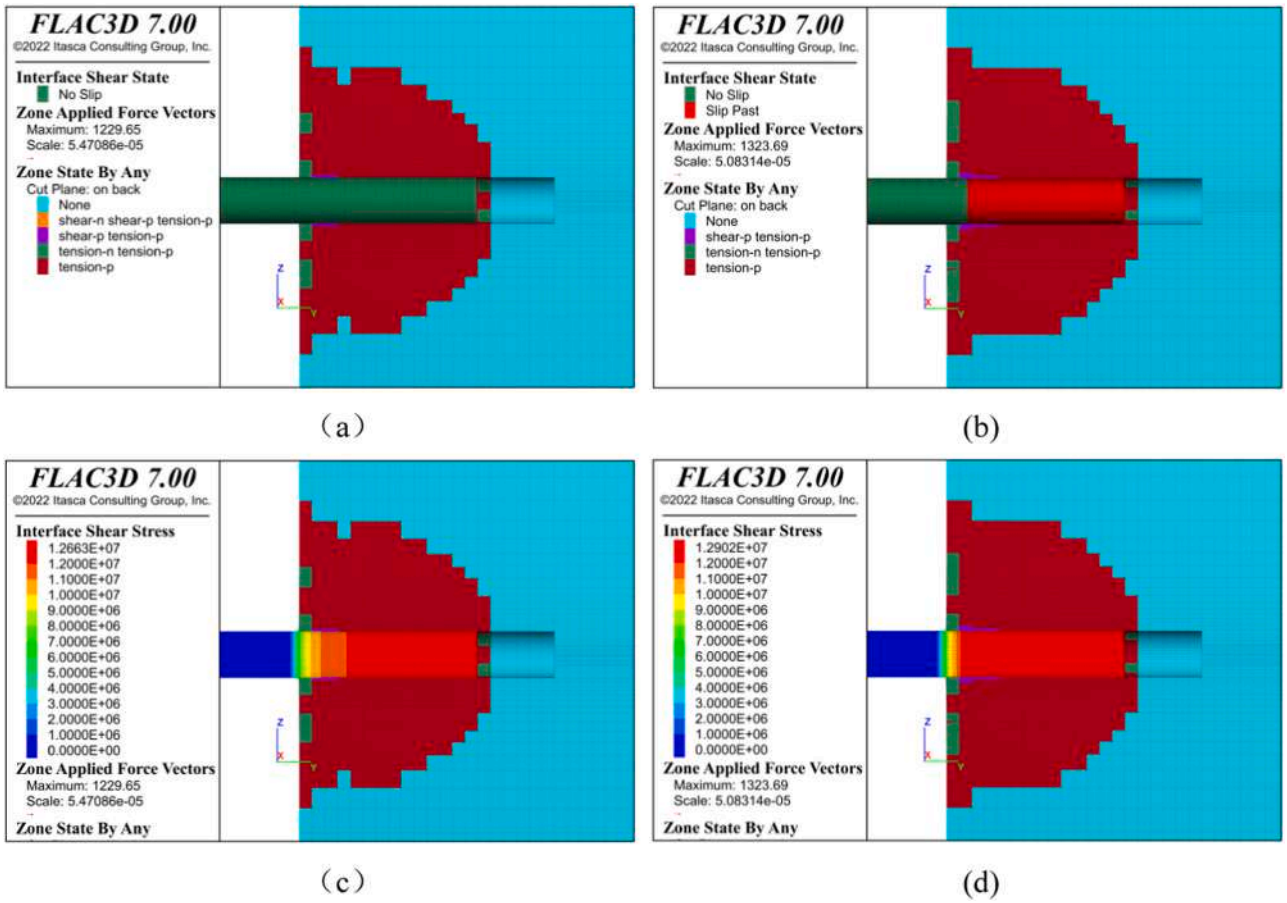

Fig. 14. The state condition and shear stresses in the interface when the applied axial force is equal to 228.7 kN to 246.2 kN. Key: Figures (a) and (c) refer to the state condition and shear stresses on the interface separately, when the applied tensile force is 228.7 kN; figures (b) and (d) are same for an axial force of 246.2 kN.

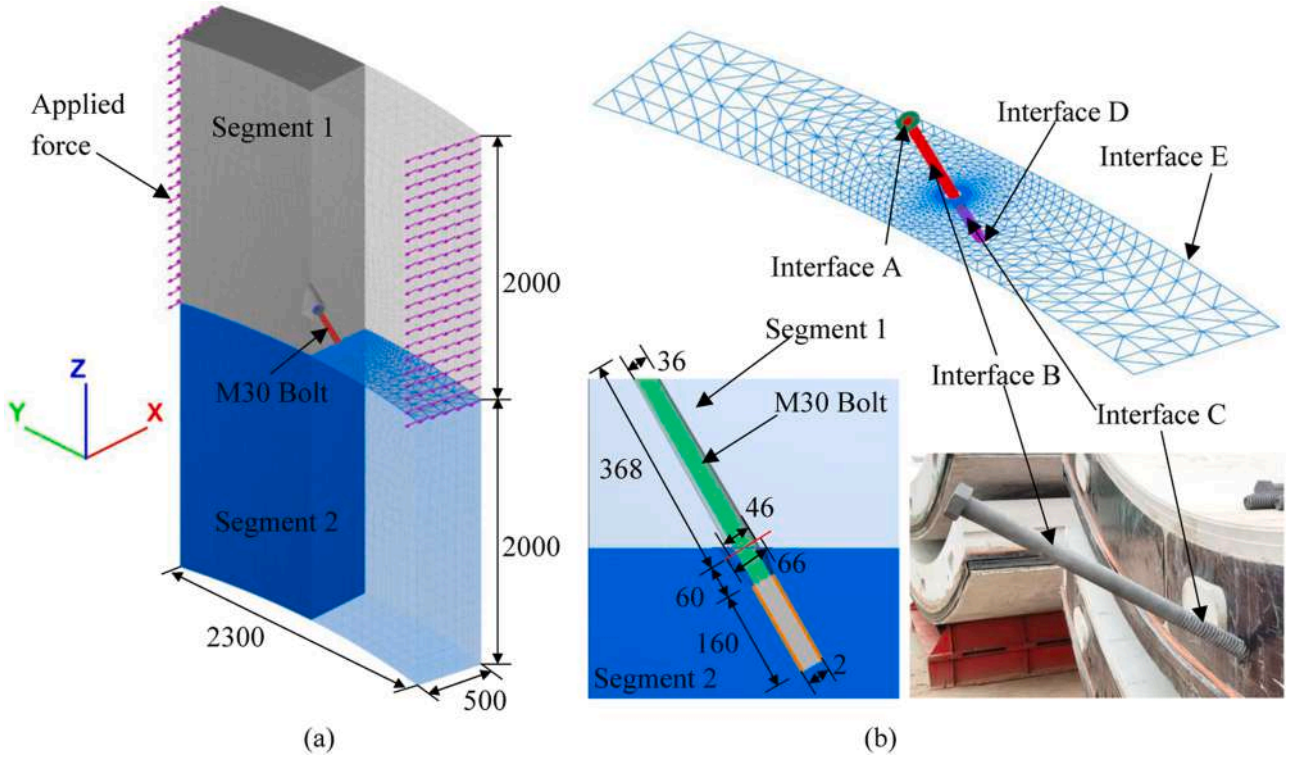

Fig. 15. Size of the developed numerical model and main characteristics of the elements and interfaces that were considered. Key: (a) the segmental lining joint with the relative shear force applied on the circular joint; (b) the details of the main elements and interfaces. (Interface A is between the bolt head and the concrete; Interface B is attached to the surface on the bolt shank; Interface C is the one on the thread part of the bolt; Interface D is on the bottom of the bolt.

Table 4
Adopted parameters for the interface C of the model.

Normal stiffness (MPa)	Shear stiffness (MPa)	Cohesion (MPa)	Friction (°)	Tensile strength (MPa)
10^5	10.1×10^3	14.7	0	14.7

Table 5
Adopted parameters for the bolt steel and concrete.

Material	Young's Modulus (GPa)	Poisson's ratio	Cohesion (MPa)	Friction (°)	Tensile strength (MPa)
Bolt	210	0.3	416	0.0001	832
Concrete	35	0.2	18.23	41	3.5

starts from the slip of the Interface C, and the plastic zone is mainly developed around the bolt due to the tensile stresses. The shear yielding of the concrete is developed near the segmental lining joint, the bolt head and the connection location between the shank and the thread part. In the no-tensile behavior, there is no tensile stress in the bolt (Fig. 17), and no slippage on the interface. The yielding of the joint is mainly caused by the bolt and concrete yielding. It is obvious that the plastic zone developes in the zone compressed by the bolt. The yielding of the compressed zones is due to tensile stresses; the plastic zones caused by shear stresses are larger than the ones due to tensile stresses and they are distributed around the segmental lining joint. Moreover, there is a great difference in the dislocation when the applied shear force is the same: the joint has a larger dislocation for the no-tensile behavior, it means that when the bolt is stretched, there is a low dislocation along the joint. Therefore, the limit dislocation of the joint is different for the two possible relative displacements (negative or positive) parallel to the circumferential joint.

Therefore, on the basis of the previous comments, when the deformation of the joint follows the tensile behavior, the tensile strength of concrete around the bolt needs to be improved and the shear strength on the composite structure among the bolt-sleeve and concrete needs to be controlled. However, when the joint deformation follows the no-tensile behavior, the compressed zone under the bolt needs to be focused.

In Fig. 17, The results show that the numerical model has similar yielding locations with the test results, where the yielding zone mainly develops near the connection between the shank and thread part of the bolt; another one is near the joint. With the same applied shear force, the plastic zones only develop near the connection between the shank and thread of bolt.

Therefore, the bolt in the tensile behavior is stretched and sheared when the segments have a certain dislocation along the joint, and the applied shear force is balanced by tensile and shear stresses in the bolt. The tensile behavior induces a higher stiffness of the joint than the no-tensile one.

During the tunnel construction, the segmental lining has an upward displacement under the application of buoyancy forces. The bolts in the circular joint have different behaviours. For example, on the basis of the installation methods of inclined bolts for the connection of rings and segments, the deformation of the bolt in the top part of the lining rings refers to the no-tensile behavior: the bolt yielding due to the shear stresses develops and the concrete tensile yielding needs to be paid attention.

He et al. [27] were able to obtain the curves of the applied shear force varying the relative displacement by the laboratory experimentation; in Fig. 18 these curves are shown together with the calculation results obtained by the tridimensional numerical calculation. In the numerical model the friction between the segments is ignored and for this reason, on the basis of the test measures, an initial value of 300 kN is added to the applied shear forces for the curves representing the calculation results.

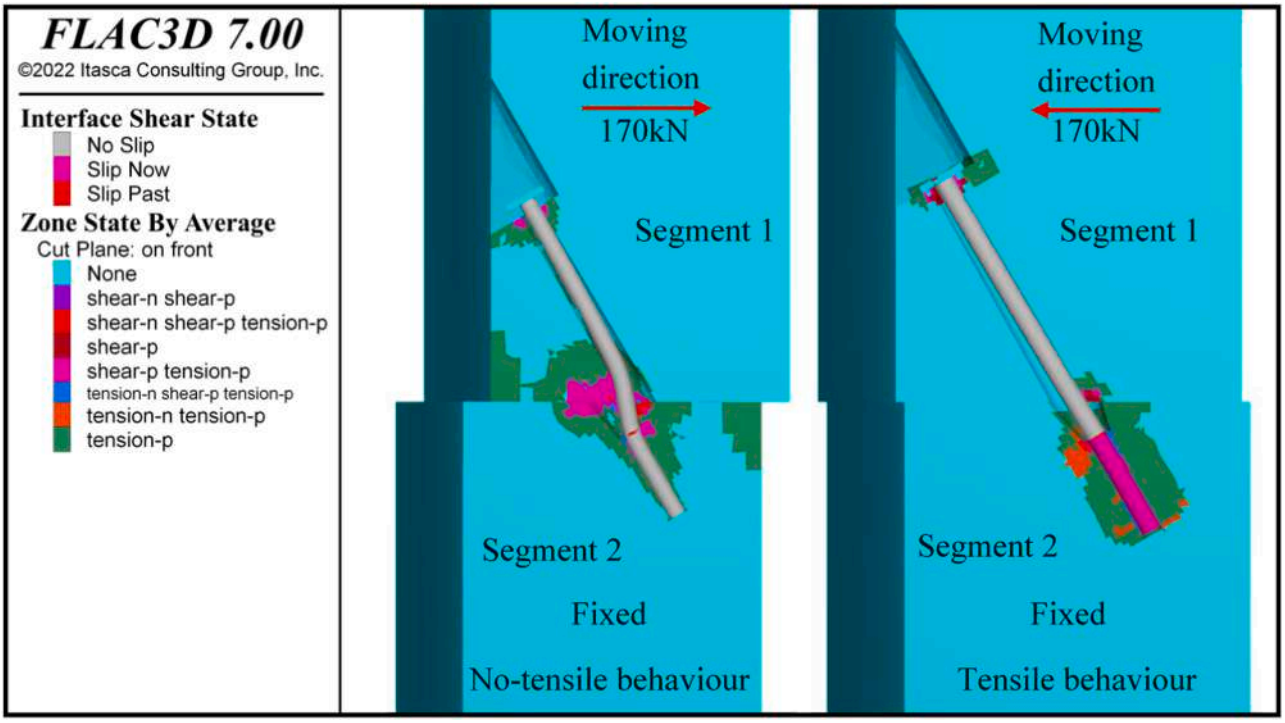

Fig. 16. The state condition of the joint including concrete, bolt and interfaces. Key: the contour of the bolt represents the state condition of the interface between the bolt and the bolt hole (Interfaces B and C).

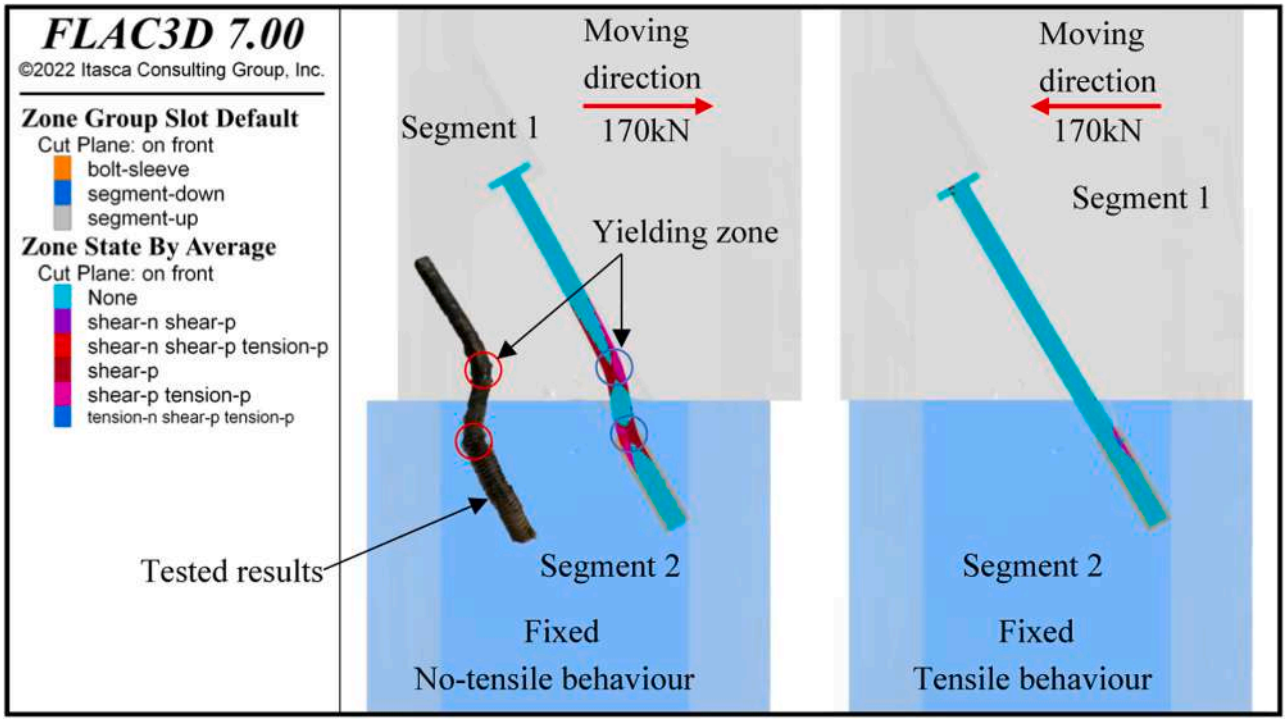

Fig. 17. The state of the bolt. Key: tested results of He et al. [27].

For the tensile behavior, the numerical results show a similar trend with the test measures at the first stage (Fig. 18). When the applied shear force reaches 220 kN, there is an obvious increase of the relative displacements along the joint. The state condition among the concrete and the interfaces is shown in Fig. 19. It is clearly shown that the interface starts to slip when the applied shear force is equal to 240 kN, but the bolt does not contact the hole wall in Segment 1. When the applied shear force reaches 260 kN, the bolt completely contacts Segment 1, and this causes the increase of the loading capacity of the joint again. The shear strength of the bolt-sleeve/concrete composite structure has a significant influence on the shear deformation of the segmental lining joint (circular joint).

For the no-tensile behavior (Fig. 18), there is a significant increase of the relative shear displacement with low shear forces at the first stage,

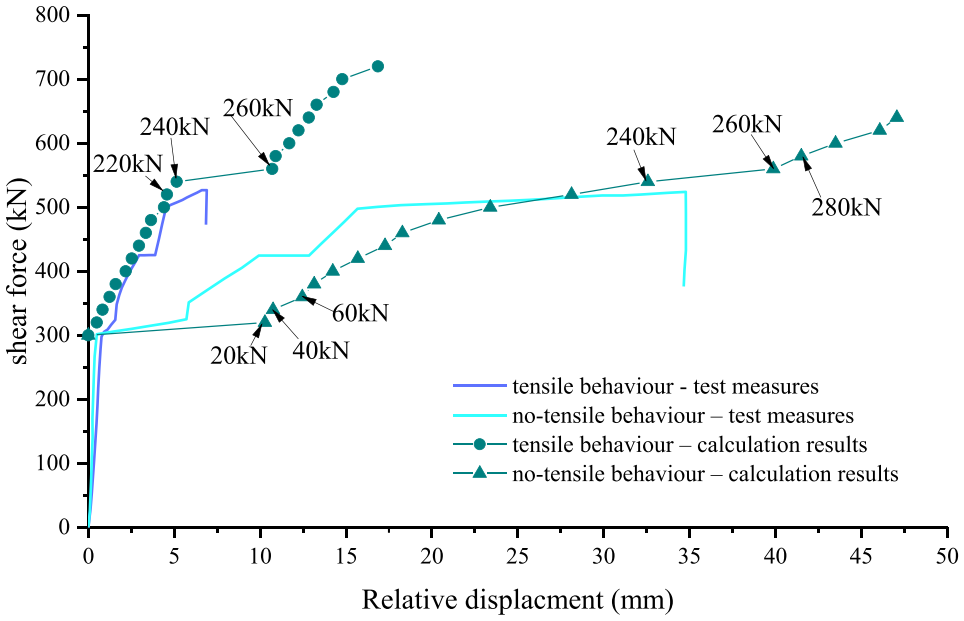

Fig. 18. Comparison of the curves of the applied shear forces varying the relative displacements, obtained by the numerical model results and by the laboratory test measures of He et al. [27].

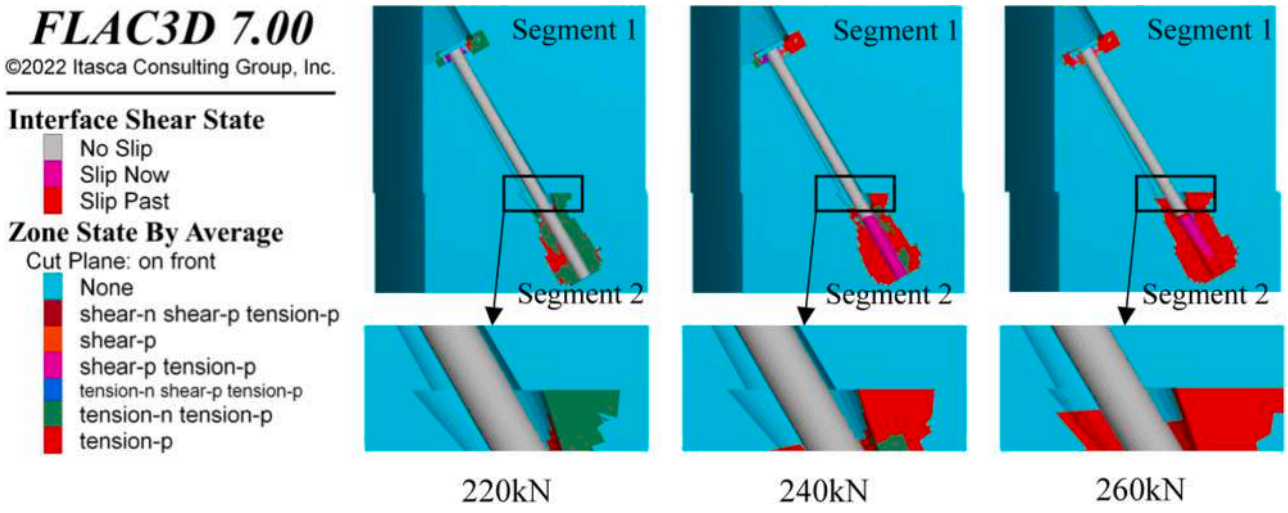

Fig. 19. The development of the plastic zones of the concrete and interfaces for different shear forces (220 kN, 240 kN, 260 kN) applied to the circular joint. Key: the interaction among the segments and the bolt is partially amplified.

and then a stable increase of the shear forces with the increase of the relative displacements of the segments along the joint. At the beginning of the shear deformation of the bolt, the contact model between the bolt and the hole wall changes with the increase of the applied shear force (Fig. 20). Since there is not any tensile force in the bolt, the bolt contacts with the hole wall in the opposite side of the movement direction of Segment 1; the contact of the bolt changes to the other side under the application of the constraints from the concrete. Since the contact zone between the bolt and concrete is not smooth, a plastic zone develops in the concrete, and this clearly shows the interaction between the bolt and concrete on the hole wall.

In Fig. 18, the increasement of the relative displacement of segments produces an increase of the applied shear forces due to the extension of the plastic zones: it means that the joint become softening. A good consistency between the test measures and the calculation results obtained by the numerical model can be found. For the no-tensile behavior, the yielding of the concrete determines the yielding of the segmental lining joint. Additionally, there is a slight increase of the curves when the applied shear force is larger than 260 kN: the main reason is due to the contact between the bolt and the hole wall of Segment 2 near the joint (Fig. 21).

On the other hand, there are some differences between the test results and the calculated ones. From the results of the numerical simulation, the shift of the contact relationship between the bolt and bolt hole causes the change of the curves due to the yield of the materials. However, there is an initial value of shear force which is undertaken by the friction of the joint interface in the laboratory test, which may be released and lead to the yield of the joint when there is an obvious relative displacement due to the materials yielding.

6. Discussion and conclusions

The shear stiffness influences the shear behavior of the circular joint when the rings of a tunnel segmental lining have a relative movement

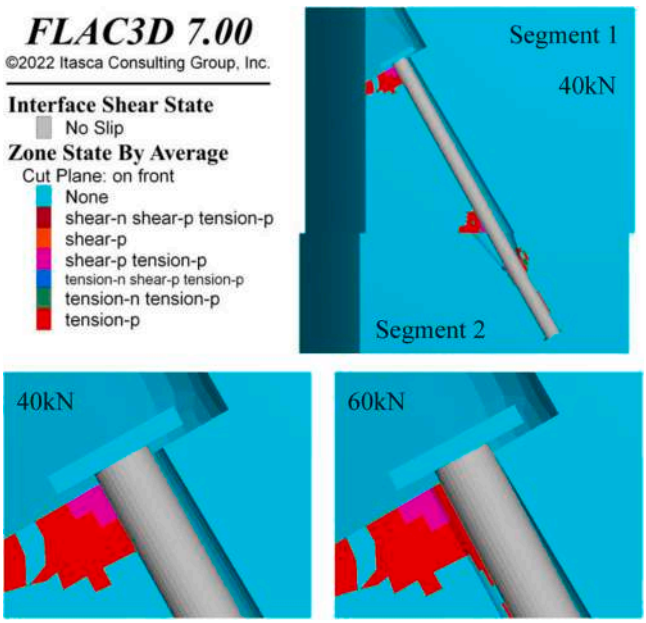

Fig. 20. The change of the contact zone between the bolt and the concrete on the hole wall, for two different applied shear forces (40 kN and 60 kN).

(dislocation); in this paper detailed 3D numerical models were developed to study this aspect and obtain interesting information necessary to perform calculations and reach a correct design of the segmental lining.

An important device for connecting segments and lining rings is the steel bolt. Its behavior must be studied in detail inside the hole because has effects on the shear deformation (and shear stiffness) of the circular joint.

In order to calibrate the 3D numerical models, the material parameters at a very little scale of the interaction between the bolt and concrete on the hole wall, were evaluated by a back analysis procedure thanks to available laboratory experiments specifically developed to this aim. Based on the results of the back analysis, the compression strength of the concrete and the bolt yielding strength have both a great influence on the shear stiffness of the lining joint. Considering the size effect, the concrete compression strength is about 2 times the standard value, and the bolt yielding strength is about 1.3 times the standard one. It was confirmed that the scale effect is very important when simulating the connecting bolt deformation inside its hole.

On the basis of the obtained calibrated parameters, the bolt deformation under an applied shear force in the cross section of the hole is analyzed, and equations for the concrete compressive foundation modulus on the hole wall are proposed and compared with the existing ones in the scientific literature: a good consistence was found. Due to the nonlinear behavior of the materials, the value of the concrete compressive foundation modulus shows a nonlinear trend, where the value decrease with the increase of the applied force. Furthermore, the influence on the concrete compressive foundation modulus of the diameter of the bolt hole and the location of the bolt in the cross section is discussed. Particularly, it was found how the constraints on the bottom of the model has a great influence on the bolt displacement.

For the shear deformation of the composite structure which is composed of the bolt, sleeve and concrete, a 3D model was developed on the basis of performed pull-out tests. Thanks to the analyzed results, for the shear foundation modulus at the interface of bolt-sleeve/concrete, a value of 10.1 MPa/mm was suggested; moreover, on the same interface a cohesion of 14.7 MPa was proposed.

Finally, a detailed 3D model of the segmental lining joint with an inclined connecting bolt was developed, adopting the material and interface parameters found in the above part of the paper. Two main types of joint shear deformation were detected: a no-tensile behavior and a tensile behavior. In the no-tensile behavior, there is no any compression force on the bolt head; on the contrary, the bolt head is compressed by the concrete structure in the tensile behavior. Correspondingly, there are obvious differences between these two behaviors: the bolt with a no-tensile behavior has a great bending deformation, and two plastic zones can be found near the joint when the joint is close to its limit condition. The yielding of the bolt-sleeve/concrete interface is the main characteristic when the joint deformation tends to its limit. The calculated results showed good agreement with test measures performed in laboratory experimentations.

When evaluating the shear stiffness of segmental lining joint, it is important to determine the contribution of the bolts based on the locations of the bolts on the circular joint. For the further research, the detailed calculation method needs to be discussed considering the nonlinear behavior of each bolt with the relative displacement of the joint.

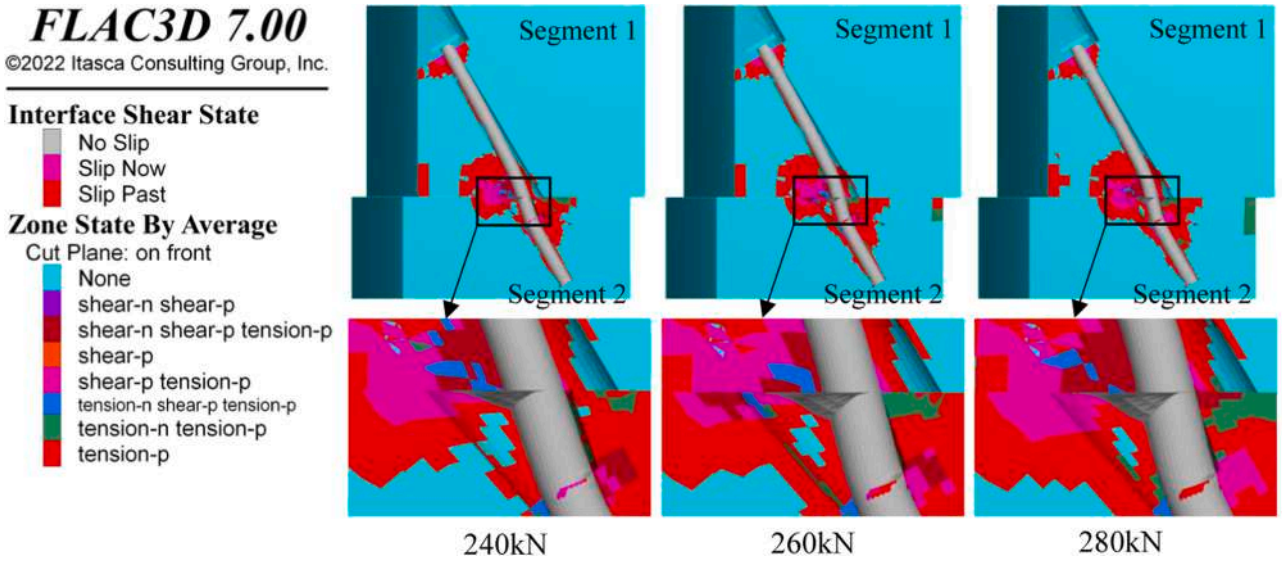

Fig. 21. The development of plastic zones at the contact area between the bolt and concrete near the joint. Key: the interaction among the segments and the bolt is partially amplified.

Declaration of Competing Interest

The authors declare that they have no known competing financial interests or personal relationships that could have appeared to influence the work reported in this paper.

Data availability

No data was used for the research described in the article.

Acknowledgements

This study was financially supported by the National Natural Science Foundation of China (No. 52378389), and this support is gratefully acknowledged. The first author also would like to appreciate the scholarship from China Scholarship Council (Grant No. 202106560030) for his study in Politecnico di Torino.

References

[1] Gong QM, Zhao Y, Zhou JH, Zhou SH. Uplift resistance and progressive failure mechanisms of metro shield tunnel in soft clay. Tunn Undergr Space Technol 2018; 82:222–34.
[2] Krahl PA, Palomo II, Almeida SJdC, Henrique Siqueira G, Pinto Júnior NdO, Vieira Junior LCM. Tolerances for TBM thrust load based on crack opening performance of fiber-reinforced precast tunnel segments. Tunn Undergr Space Technol 2021; 111.
[3] Li X, Di H, Zhou S, Huo P, Huang Q. Effective method for adjusting the uplifting of shield machine tunneling in upper-soft lower-hard strata. Tunn Undergr Space Technol 2021;115.
[4] Nogales A, de la Fuente A. Crack width design approach for fibre reinforced concrete tunnel segments for TBM thrust loads. Tunn Undergr Space Technol 2020; 98.
[5] Zhou SH, Ji C. Tunnel segment uplift model of earth pressure balance shield in soft soils during subway tunnel construction. Int J Rail Transp 2014;2:221–38.
[6] Gan X, Yu J, Gong X, Zhu M. Characteristics and countermeasures of tunnel heave due to large-diameter shield tunneling underneath. J Perform Constr Facil 2020;34.
[7] Jin D, Yuan D, Ng YCH, Pan Y. Effect of an undercrossing tunnel excavation on an existing tunnel considering nonlinear soil-tunnel interaction. Tunn Undergr Space Technol 2022;130.
[8] Zaheri M, Ranjbarnia M, Dias D. 3D numerical investigation of segmental tunnels performance crossing a dip-slip fault. Geomech Eng 2020;23:351–64.
[9] Zaheri M, Ranjbarnia M, Dias D, Oreste P. Performance of segmental and shotcrete linings in shallow tunnels crossing a transverse strike-slip faulting. Transp Geotech 2020;23.
[10] Feng H, Ye F, Jiang Y, Wang J, Wen X, Fang Q. Effect of rolling angle on segment cracking and damage of shield tunnel - field investigation and modelling. Eng Fail Anal 2022;140.
[11] Han L, Ye G-l, Chen J-j, Xia X-h, Wang J-h. Pressures on the lining of a large shield tunnel with a small overburden: A case study. Tunn Undergr Space Technol 2017; 64:1–9.
[12] Liu DJ, Tian C, Wang F, Hu QF, Zuo JP. Longitudinal structural deformation mechanism of shield tunnel linings considering shearing dislocation of circumferential joints. Comput Geotech 2021;139:15.
[13] Mo HH, Chen JS. Study on inner force and dislocation of segments caused by shield machine attitude. Tunn Undergr Space Technol 2008;23:281–91.
[14] Wang M, Dong Y, Yu L, Fang L, Wang X, Liu D. Experimental and numerical researches of precast segment under radial dislocation conditions. Tunn Undergr Space Technol 2019;92.
[15] Wang S, Liu C, Shao Z, Ma G, He C. Experimental study on damage evolution characteristics of segment structure of shield tunnel with cracks based on acoustic emission information. Eng Fail Anal 2020;118.
[16] Zheng G, Sun J, Zhang T, Zhang X, Cheng H, Wang H, Diao Y. Mechanism and countermeasures of progressive failure in shield tunnels. Tunn Undergr Space Technol 2023;131.
[17] Huang LC, Ma JJ, Lei MF, Liu LH, Lin YX, Zhang ZY. Soil-water inrush induced shield tunnel lining damage and its stabilization: A case study. Tunn Undergr Space Technol 2020;97:16.
[18] Liu DJ, Wang F, Hu QF, Huang HW, Zuo JP, Tian C, Zhang DM. Structural responses and treatments of shield tunnel due to leakage: A case study. Tunn Undergr Space Technol 2020;103:18.
[19] Gue CY, Wilcock M, Alhaddad MM, Elshafie MZEB, Soga K, Mair RJ. The monitoring of an existing cast iron tunnel with distributed fibre optic sensing (DFOS). J Civ Struct Health Monit 2015;5:573–86.
[20] Wu HN, Shen SL, Liao SM, Yin ZY. Longitudinal structural modelling of shield tunnels considering shearing dislocation between segmental rings. Tunn Undergr Space Technol 2015;50:317–23.
[21] Zheng G, Zhang X, Zhang T, Sun J, Qiu H, Diao Y. Numerical study on mechanical behavior and ultimate bearing capacity of shield segment joints under different load conditions. Tunn Undergr Space Technol 2023;139.
[22] Zhu H, Wang D, Shi B, Wang X, Wei G. Performance monitoring of a curved shield tunnel during adjacent excavations using a fiber optic nervous sensing system. Tunn Undergr Space Technol 2022;124.
[23] Gue CY, Wilcock MJ, Alhaddad MM, Elshafie MZEB, Soga K, Mair RJ. Tunnelling close beneath an existing tunnel in clay – perpendicular undercrossing. Géotechnique 2017;67:795–807.
[24] Chen RP, Meng FY, Ye YH, Liu Y. Numerical simulation of the uplift behavior of shield tunnel during construction stage. Soils Found 2018;58:370–81.
[25] Han X, Oreste P, Ye F. The buoyancy of the tunnel segmental lining in the surrounding filling material and its effects on the concrete stress state. Geotech Geol Eng 2023;41:741–58.
[26] Han X, Oreste P, Ye F. The important role of stiffnesses values of circular joints on the stress state developed in the tunnel segmental lining. Geomech Geophys Geo-Energy Geo-Resour 2023;9(1):32.
[27] He Y, Yang Z, Liu X, Ding W. Theoretical solution for failure mechanism of circumferential joint of shield tunnel segment connected using diagonal bolts. Tunn Constr 2021;41.
[28] Li D, Chen Z, Yang Z. Test and analysis of shear performance of Circumferential joint of segment ring. Undergr Eng Tunn 2011:15–7.
[29] Liu X, Dong ZB, Song W, Bai Y. Investigation of the structural effect induced by stagger joints in segmental tunnel linings: Direct insight from mechanical behaviors of longitudinal and circumferential joints. Tunn Undergr Space Technol 2018;71:271–91.
[30] Putke T, Bohun R, Mark P. Experimental analyses of an optimized shear load transfer in the circumferential joints of concrete segmental linings. Struct Concr 2015;16:572–82.
[31] Zuo L, Zhang J, Feng K, Yang W, Zhang L, He C. Experimental study on Inter-ring joint shearing characteristics of gas transmission shield tunnel with bent bolt and tenon. Tunn Undergr Space Technol 2022;130.
[32] Chen Y, Li CC. Performance of fully encapsulated rebar bolts and D-Bolts under combined pull-and-shear loading. Tunn Undergr Space Technol 2015;45:99–106.
[33] Chen Y, Wen G, Hu J. Analysis of Deformation Characteristics of Fully Grouted Rock Bolts Under Pull-and-Shear Loading. Rock Mech Rock Eng 2020;53:2981–93.
[34] Jalalifar H, Aziz N. Experimental and 3D Numerical Simulation of Reinforced Shear Joints. Rock Mech Rock Eng 2009;43:95–103.
[35] Jalalifar H, Aziz N, Hadi M. The effect of surface profile, rock strength and pretension load on bending behaviour of fully grouted bolts. Geotech Geol Eng 2006;24:1203–27.
[36] Sørensen JH, Hoang LC, Olesen JF, Fischer G. Testing and modeling dowel and catenary action in rebars crossing shear joints in RC. Eng Struct 2017;145:234–45.
[37] Takase Y. Testing and modeling of dowel action for a post-installed anchor subjected to combined shear force and tensile force. Eng Struct 2019;195:551–8.
[38] He L, An XM, Zhao XB, Zhao ZY, Zhao J. Development of a Unified Rock Bolt Model in Discontinuous Deformation Analysis. Rock Mech Rock Eng 2017;51:827–47.
[39] Li X, Nemcik J, Mirzaghorbanali A, Aziz N, Rasekh H. Analytical model of shear behaviour of a fully grouted cable bolt subjected to shearing. Int J Rock Mech Min Sci 2015;80:31–9.
[40] Ma S, Zhao Z, Nie W, Zhu X. An Analytical Model for Fully Grouted Rockbolts with Consideration of the Pre- and Post-yielding Behavior. Rock Mech Rock Eng 2017; 50:3019–28.
[41] Oreste PP, Cravero M. An analysis of the action of dowels on the stabilization of rock blocks on underground excavation walls. Rock Mech Rock Eng 2008;41: 835–68.
[42] Liao SM, Peng FL, Shen SL. Analysis of shearing effect on tunnel induced by load transfer along longitudinal direction. Tunn Undergr Space Technol 2008;23: 421–30.
[43] Cheng HZ, Chen RP, Wu HN, Meng FY, Yi YL. General solutions for the longitudinal deformation of shield tunnels with multiple discontinuities in strata. Tunn Undergr Space Technol 2021;107.
[44] Liang RZ, Xia TD, Huang MS, Lin CG. Simplified analytical method for evaluating the effects of adjacent excavation on shield tunnel considering the shearing effect. Comput Geotech 2017;81:167–87.
[45] Shi CH, Wang ZX, Gong CJ, Liu JW, Peng Z, Cao CY. Prediction of the additional structural response of segmental tunnel linings induced by asymmetric jack thrusts. Tunn Undergr Space Technol 2022;124:19.
[46] Wu HN, Shen SL, Yang J, Zhou AN. Soil-tunnel interaction modelling for shield tunnels considering shearing dislocation in longitudinal joints. Tunn Undergr Space Technol 2018;78:168–77.
[47] Han X, Oreste P, Ye F. The contribution of the bolting system to the shear stiffness of circumferential joints in tunnel segmental linings. Comput Geotech 2023;162: 1–21.
[48] Han X, Oreste P, Ye F. The influence of the nonlinear behaviour of connecting bolts on the shear stiffness of circular joints in a tunnel segmental lining. Tunn Undergr Space Technol 2024;146:1–27.
[49] Khazaee A, Ghalehnovi M. Bearing Stiffness of UHPC; An Experimental Investigation and A Comparative Study of Regression and SVR-ABC Models. J Adv Concr Technol 2018;16:145–58.
[50] Soroushian P, Obaseki K, Rojas MC. Bearing strength and stiffness of concrete under reinforcing bars. Acids Mater J 1987;84:179–84.
[51] Vintzēleou EN, Tassios TP. Mathematical models for dowel action under monotonic and cyclic conditions. Mag Concr Res 1986;38:13–22.
[52] Poli SD, Prisco MD, Gambarova PG. Shear response, deformations, and subgrade stiffness of a dowel bar embedded in concrete. Acids Struct jourrnal 1992:665–75.
[53] Figueira D, Sousaa C, Nevesb AS. Winkler spring behavior in FE analyses of dowel action in statically loaded RC cracks. Comput Concr 2018;21:593–605.

[54] Li P-F, An X-H, He S-Q, Chen C. Three-dimensional bond model considering the coupled damage effect for dowel action. Mag Concr Res 2017;69:728–44.
[55] Ma S, Zhao Z, Shang J. An analytical model for shear behaviour of bolted rock joints. Int J Rock Mech Min Sci 2019;121.
[56] Maekawa K, Qureshi J. Computational Model for Reinforcing Bar Embedded in Concrete under Combined Axial Pullout and Transverse Displacement. J Mater, Conc Struct 1996;31:227–39.
[57] Maekawa K, Qureshi J. Stress transfer across interfaces in reinforced concrete due to aggregate interlock and dowel action. J Mater, Conc Struct 1997;34:159–72.
[58] Mannava SS, Bush Jr TD, Kukreti AR. Load-deflection behavior of smooth dowels. Acids Struct J 1999;96:891–9.
[59] Moradi AR, Soltani M, Tasnimi AA. A Simplified Constitutive Model for Dowel Action across RC Cracks. J Adv Concr Technol 2012;10:264–77.
[60] Poli SD, Prisco MD, Gambarova PG. Cover and stirrup effects on the shear response of dowel bar embedded in concrete. Acids Struct jourrnal 1993:441–50.
[61] Soltani M, An X, Maekawa K. Computational model for post cracking analysis of RC membrane elements based on local stress–strain characteristics. Eng Struct 2003; 25:993–1007.
[62] Soltani M, An X, Maekawa K. Cracking response and local stress characteristics of RC membrane elements reinforced with welded wire mesh. Cem Concr Compos 2004;26:389–404.
[63] Soroushian P, Obaseki K, Rojas MC. Behavior of bars in dowel action against concrete cover. Acids Mater J 1987;84:179–84.
[64] ACI Committee 325. Structural design considerations for pavement joints. J Am Concr Inst 1956;53:1–28.
[65] Yin W, Lu H, Yuan J, Huang B. Mechanical characteristics of dowel bar-concrete interaction: based on substructure experiment. Int J Pavement Eng 2022;23: 2392–404.
[66] Conforti A, Tiberti G, Plizzari GA. Splitting and crushing failure in FRC elements subjected to a high concentrated load. Compos Part B: Eng 2016;105:82–92.
[67] Markić T, Morger F, Kaufmann W. Partially loaded areas in reinforced concrete: Mechanical modelling. Eng Struct 2022;271.
[68] Markić T, Morger F, Kaufmann W. Partially loaded areas in reinforced concrete: Experimental campaign and model validation. Eng Struct 2022;273.
[69] Oreste P. Back-analysis techniques for the improvement of the understanding of rock in underground constructions. Tunn Undergr Space Technol 2005;20:7–21.
[70] Walton G, Sinha S. Challenges associated with numerical back analysis in rock mechanics. J Rock Mech Geotech Eng 2022;14:2058–71.
[71] Geng P, Wang Q, Guo X, Zeng G, Chen C, He C. Pull-out test of longitudinal joints of shield tunnel. China J Highw Transp 2020;33:124–34.
[72] Itasca Consulting Group, 2023. Itasca's FLAC3D Documentation.